Proceedings of the Hydraulic Machinery and Systems 21st IAHR Symposium
September 9-12, 2002, Lausanne

VALIDATIONS AND INVESTIGATIONS OF THE COMPUTED FLOW IN THE GAMM FRANCIS RUNNER AND THE HÖLLEFORSEN KAPLAN RUNNER

Håkan NILSSON, *CHALMERS/Thermo and Fluid Dynamics, SE – 412 96 Gothenburg, Sweden*

Lars DAVIDSON, *CHALMERS/Thermo and Fluid Dynamics, SE – 412 96 Gothenburg, Sweden*

ABSTRACT

The parallel multiblock finite volume CFD code CALC-PMB is used for computing the turbulent flow in the GAMM Francis runner and the Hölleforsen Kaplan runner at best and off-design operating conditions. The computational results are validated against detailed measurements and observations. A general method for estimating numerical accuracy in swirling flow, based on the conservation of angular momentum, is applied. The Kaplan tip vortex is investigated and compared at two operating conditions. The use of surface restricted streamlines (smearlines) to locate important flow features is investigated.

RÉSUMÉ

Le code CFD volumes finis parallèle multi bloc CALC-PMB est utilisé pour modéliser l'écoulement turbulent dans la roue Francis GAMM et dans la roue Kaplan Hölleforsen aux points de fonctionnement nominal et hors nominal. Les résultats numériques sont validés par des mesures et des observations détaillées. Une méthode générale basée sur la conservation de la quantité de mouvement angulaire est utilisée pour estimer l'exactitude du calcul numérique dans l'écoulement tourbillonnaire. Le tourbillon marginal dans une turbine Kaplan est étudié et comparé pour deux points de fonctionnement. Des lignes de courants limitées à la surface sont utilisées pour localiser les caractéristiques importantes de l'écoulement.

INTRODUCTION

This work investigates finite volume CFD (Computational Fluid Dynamics) results of the flow in two different kinds of water turbine runners and compares the computational results with detailed experimental results and observations. The accuracy of the computational results is further investigated with a general method for estimating numerical accuracy in swirling flow, based on the conservation of angular momentum [6, 11].

The runners studied are the GAMM Francis runner model and the Hölleforsen Kaplan runner model. The GAMM Francis runner was used as a test case in the 1989 *GAMM Workshop on 3D Computation of Incompressible Internal Flows* [14], where the geometry and detailed best efficiency measurements were made available. In addition to the best efficiency measurements, four off-design operating condition measurements have been made.

The Hölleforsen Kaplan runner was used at the 1999 *Turbine 99* and 2001 *Turbine 99 - II* workshops on draft tube flow [1], where detailed measurements made after the runner were used as inlet boundary conditions for the draft tube computations. This work uses the measurements

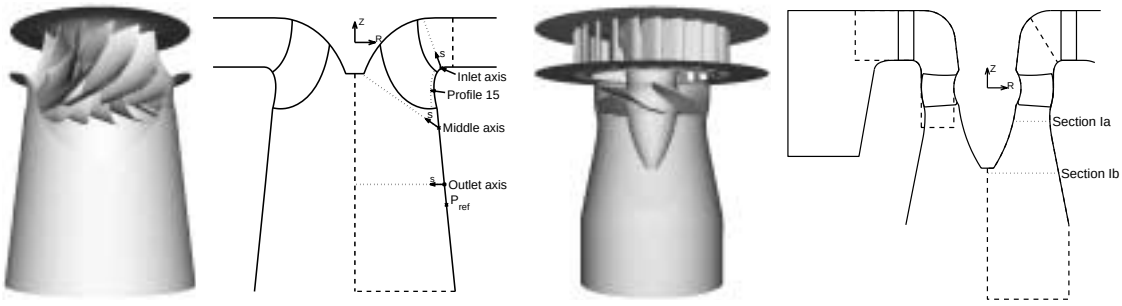

(a) GAMM geometry. (b) GAMM schematic meridional description. (c) Hölleforsen geometry. (d) Hölleforsen schematic meridional description.

Figure 1: The GAMM Francis runner and Hölleforsen Kaplan runner geometries, meridional contour (solid lines) and the domains computed (dashed lines). The left domain of the Hölleforsen description (d) is the guide vane domain, with a radial inlet in the spiral casing region and an axial outlet in the runner region. The right domains are the runner domains, with a radial inlet at the top and an axial outlet at the bottom. The dotted lines are sections in which the results are compared with measurements. Note that the GAMM inlet boundary conditions are extrapolated from the measured inlet axis to the inlet of the computational domain.

Operating point	Volume flow rate coefficient $[-]$ $\varphi = \frac{Q}{\pi \Omega R_{ref}^3}$	Energy coefficient $[-]$ $\psi = \frac{2E}{\Omega^2 R_{ref}^2}$	Efficiency $[-]$ $\eta = \frac{T\Omega}{\rho Q E}$
1	0.286	1.07	0.920
2	0.220	0.66	0.850
3	0.330	1.40	0.910
4	0.220	1.07	0.885
5	0.330	1.07	0.905

Table 1: The GAMM operating points, where operating point 1 is the best efficiency operating point.

at best efficiency to validate the computed runner flow. An off-design Hölleforsen computation has also been made for comparison.

The nomenclature used in this work is the same as that used at the workshops, which allows direct comparisons with the available measurements and facilitates understanding for those who are familiar with the nomenclatures of the workshops. Unfortunately, the nomenclatures are not the same in the two workshops, which must be kept in mind.

CASE DESCRIPTIONS

The GAMM model has 24 stay vanes, 24 guide vanes and 13 runner blades with a runner radius of $R_{ref} = 0.2m$. The Hölleforsen model has ten stay vanes, 24 guide vanes and five runner blades with a runner diameter of $D = 0.5m$. The tip clearance between the runner blades and the shroud is $0.4mm$. Figure 1 shows the geometries, the meridional descriptions, the computational domains and the measurement sections of the studied runners.

Table 1 shows the GAMM operating points studied in this work. Here $Q[m^3/s]$ is the volume flow rate, $\Omega = 52.36s^{-1}$ is the runner angular rotation, $E[J/kg]$ is the specific hydraulic energy and $T[Nm]$ is the runner torque.

The Hölleforsen *standard* case [1, 9] (test case T, which is close to best efficiency, at the Turbine 99 workshop) has diameter $D = 0.5m$, a head of $H = 4.5m$, a runner speed of

$N = 595rpm$ (unit speed $N_{11} = ND/\sqrt{H} = 140$) and a volume flow rate of $Q = 0.522m^3/s$ (unit flow $Q_{11} = Q/D^2\sqrt{H} = 0.98$). An additional Hölleforsen case is studied in this work, where the unit speed is reduced to $N_{11} = 110$. This case has a higher blade loading, which gives a stronger tip vortex (with a more unsteady behaviour that is studied in ongoing work).

The GAMM runner computations obtain the inlet boundary conditions from an extrapolation of the measurements at the measured inlet axis together with a constant inlet turbulent intensity of 5% [4, 10, 12]. The Hölleforsen runner is computed in two steps, where the circumferentially averaged flow in the guide vane computations are used as inlet boundary conditions for the runner computations. A turbulent $1/7$ profile is used as the inlet boundary condition for the guide vane computation. The choice of guide vane inlet boundary condition has been shown to affect the flow in the runner only slightly [9]. All computations are made for the steady flow at a single blade, employing rotationally periodic boundary conditions.

The GAMM grid size is $560\,736$ control volumes. The Hölleforsen grid sizes are $285\,177$ control volumes for the guide vane grid and $719\,231$ control volumes for the runner grid, where there are $15\,884$ control volumes in the tip clearance, with 19 control volumes between the runner blade tip and the shroud. The grids resolve the boundary layers to $y^+ \approx 1$, and the Low-Reynolds $k-\omega$ turbulence model of Wilcox [15], which can be integrated all the way to the wall, is used.

VALIDATION AGAINST MEASUREMENTS

The computational results are validated against detailed measurements at the measurement sections shown in figure 1. The GAMM abscissas, s, are aligned with the measurement axes and normalized by $R_{ref} = 0.2m$. The abscissa for profile 15 starts at the leading edge and follows the runner blade pressure and suction side surfaces. The GAMM velocity coefficients are normalized by $\sqrt{2E}$, and the static pressure coefficient is defined as $C_p = (P - P_{ref})/\rho E$, where E is the specific energy that can be derived from table 1 and P_{ref} is the reference static pressure (see figure 1). The Hölleforsen velocity coefficients are normalized by Q/A_i, where Q is the volume flow rate and A_i is the area of each section ($Q = 0.522m^3/s$, $A_i = 0.15m^2$ for section Ia and $A_i = 0.23m^2$ for section Ib). The normalized velocity coefficients, C_v, are the tangential (C_u, positive in the runner rotation direction), the axial (C_z, positive along the Z-axis), the radial (C_r, positive in the R-direction) and the meridional ($C_m = \sqrt{C_r^2 + C_z^2}$, always positive).

Figure 2 compares the GAMM computational results with some of the measurements [10, 12] and figure 3 compares the Hölleforsen computational results with some of the measurements [9, 12]. The computed velocity coefficients are circumferentially averaged.

It should be noted that the computations satisfy mass conservation. Thus, the disagreement in the level between the computed and measured meridional velocity distributions must originate in non-periodicity of the experimental flow, in a normalization error or in measurement errors.

All of the computational results chiefly differ from the measurements close to the axis of rotation after the runner. This is particularly true at low mass flow for the GAMM runner, where a strong unsteady vortex rope formed in the experimental set-up. Neither the computational assumptions of steady periodic flow nor the experimental method is appropriate in this region of high instabilities and recirculation. Thus better measurement techniques and numerical methods are both needed to study the flow in this region.

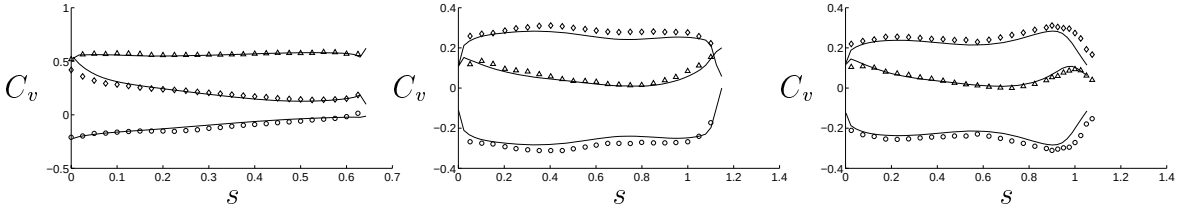

(a) Inlet axis absolute velocity coefficients, point 1.

(b) Middle axis absolute velocity coefficients, point 1.

(c) Outlet axis absolute velocity coefficients, point 1.

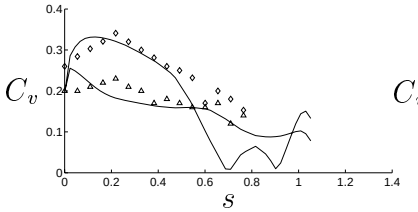

(d) Outlet axis absolute velocity coefficients, point 2.

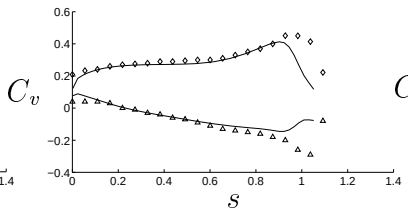

(e) Outlet axis absolute velocity coefficients, point 5.

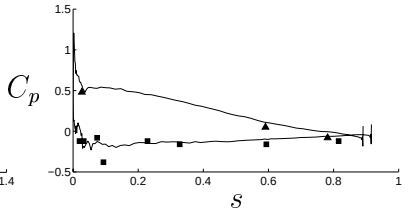

(f) Surface static pressure coefficient, profile 15, point 1.

Figure 2: GAMM flow survey. Solid lines: computational results. Measurement markers: △: Tangential; ○: Axial; ◇: Meridional; ▲: Pressure side; ■: Suction side.

NUMERICAL VALIDATION

A general numerical method for estimating numerical error in swirling flow has been developed [6, 11]. It is based on conservation of angular momentum about the axis of rotation. The imbalance in angular momentum between the inlet and any downstream surface (the numbered axi-symmetric control surfaces in figures 4(a) and 4(b)) is normalized with the inlet angular momentum and shown as a graph of the error along the main flow path [13]. The angular momentum error distributions for the cases in this work are shown in figure 4(c). The overall balance errors for the cases thus range from 0.5% to 3%. The Hölleforsen standard case is the one most thoroughly computed and investigated, which explains why it has the smallest error.

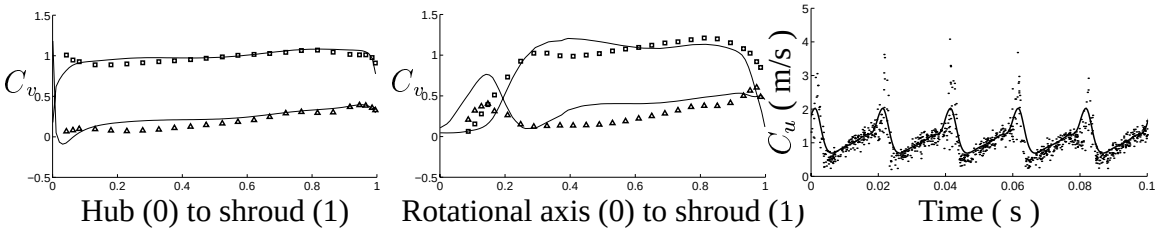

(a) Section Ia. Absolute velocity coefficients.

(b) Section Ib. Absolute velocity coefficients.

(c) Time resolved comparison at section Ia, $r^* = r/R = 0.92$, one runner revolution.

Figure 3: Hölleforsen flow survey. Solid lines: computational results. Measurement markers: △: tangential; □: meridional; dots: individual measurement samples of the tangential velocity.

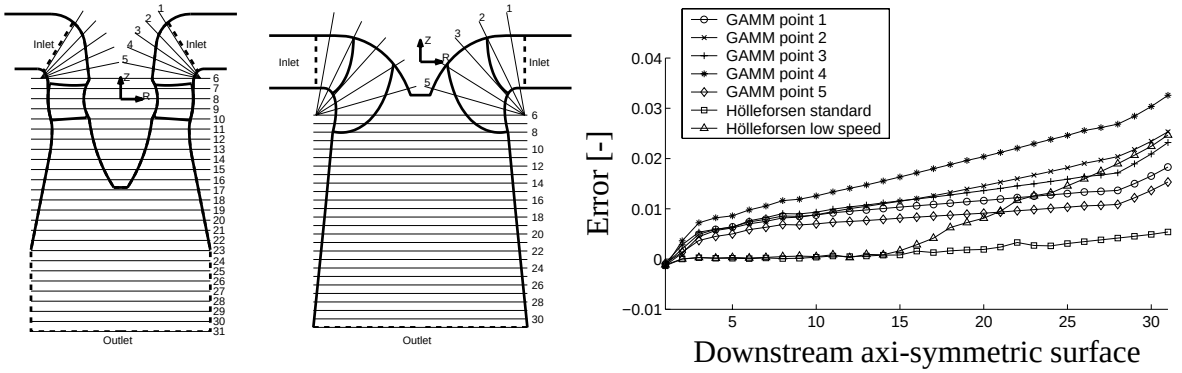

(a) Hölleforsen control surfaces.

(b) GAMM control surfaces.

(c) Angular momentum balance error.

Figure 4: Angular momentum balance error from inlet to outlet for all cases.

FLOW FEATURE VISUALIZATION

This section visualizes some of the flow features that are responsible for a reduction of the turbine efficiency. Some of the flow features, for instance the tip vortex, are also often responsible for damaging the material through cavitation formation.

The use of surface restricted streamlines (smearlines) to locate important flow features is investigated.

HÖLLEFORSEN TIP CLEARANCE FLOW

The computed flow through the $0.4mm$-wide tip clearances (all five runner blades) of the Hölleforsen runner model is $5.45 \cdot 10^{-3} m^3/s$ for the standard case, which corresponds to 1.0% of the total volume flow and $1.69 \cdot 10^{-2} m^3/s$ for the low unit speed case, which corresponds to 3.2% of the total volume flow. The tip clearance flow gives rise to a jet on the suction side of the runner blade that interacts with the shroud boundary layer and forms a vortex. Figure 5 shows streamlines that follow the flow through the tip clearance and form a suction side vortex. The vortex is small for the best efficiency operating condition but is very large for the low unit speed case. The vector plots clearly show the sizes of the vortices and the locations of the vortex cores.

The static pressure is locally reduced at the center of a vortex. This is the reason that cavitation bubbles are commonly formed in the tip vortex. Figure 6 shows iso-surfaces of the lowest computed static pressure and experimentally observed cavitational behaviour for a similar runner at roughly the same operating conditions as the computations. The best efficiency predictions in particular agree with the cavitational behaviour. The low unit speed experimental observation shows that the tip vortex cavitation starts earlier than for the best efficiency operating condition and that there is a leading edge cavity. This is qualitatively captured by the computations. It should be noted however that the computations are single phase computations that do not take cavitational effects into account.

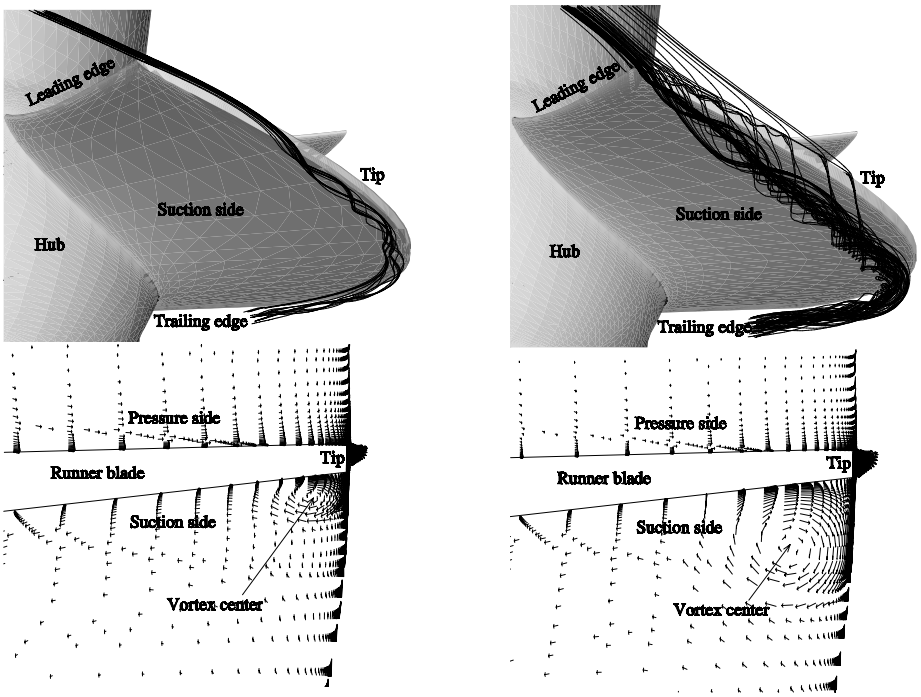

(a) Best efficiency.

(b) Low unit speed.

Figure 5: Comparison between the tip vortex size and location at the best efficiency operating condition and at a lower unit speed. The vectors are located in a meridional plane at the center of a runner blade and are projected in the main flow direction in order to magnify the secondary flow.

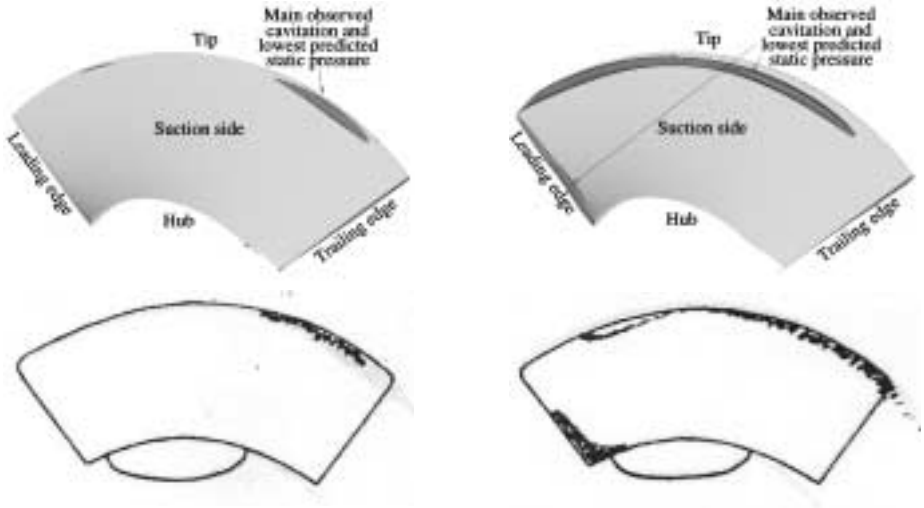

(a) Best efficiency.

(b) Low unit speed.

Figure 6: Comparison between predicted low static pressure regions (dark grey iso-surfaces) and observed cavitational behaviour at best efficiency operating condition and at a lower unit speed. The cavitational behaviour was observed in 1955 at a model test of a very similar runner at roughly the same operating conditions as the computations (Picture courtesy of GE Energy (Sweden) AB).

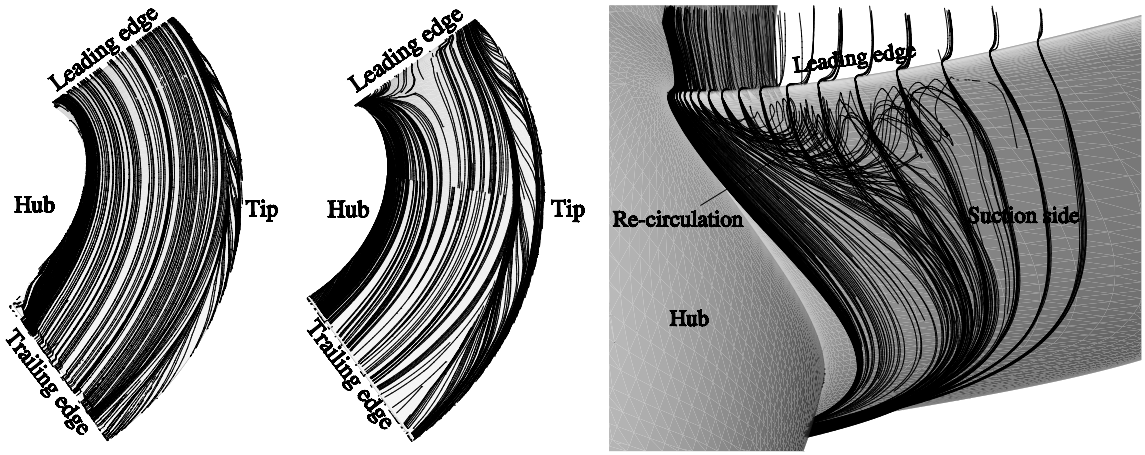

(a) Best efficiency. (b) Low unit speed. (c) Re-circulation at low unit speed.

Figure 7: Smearlines at the Hölleforsen suction side at best efficiency operating condition (a) and at low unit speed (b), and streamlines (c) visualizing a re-circulation bubble at low unit speed on the runner blade suction side close to the leading edge.

USING SMEARLINES TO FIND FLOW FEATURES

It is always a challenging task to find interesting flow features in complex flow. Vector plots are very sensitive to view angle, for instance, which makes it difficult to find even known flow features. A number of methods for feature based visualization have been presented in the literature [5]. The problem in most methods is that the definitions are not distinct, so that flow features are indicated where they should be absent, which sometimes makes the methods useless. This work shows how surface restricted streamlines (smearlines) can be used to find several flow features in water turbine runner flow. The smearlines in this work follow the streamlines that are restricted to the very first node close to the runner blade surfaces, at $y^+ \approx 1$, which augments the secondary flow features. At greater distances, the effect is much smaller. If wall functions are used instead of a low-Reynolds number turbulence model, the extra modeling introduced and the greater distance to the first node may cancel the effect. It should be recalled that rotational effects that twist the boundary layers are included in the momentum equations.

Starting with a known flow feature, the suction side smearlines of the Hölleforsen standard case (figure 7(a)) clearly show the width and distribution of the tip vortex. The suction side smearlines of the low unit speed case (figure 7(b)) show that this vortex starts earlier and is wider. These smearlines also reveal a re-circulation region at the leading edge of the blade. Once this re-circulation region was discovered, it was easily visualized in figure 7(c).

The smearline visualization method is also used to find flow features in the computed GAMM Francis runner flow. Figure 8 shows the pressure and suction side smearlines of the GAMM runner. Several as yet undiscovered flow features are easily found: separation, re-circulation, reattachment and stagnation flow. The smearline visualization is more easily understood when accompanied by common streamline visualization. Figure 9 uses common streamlines to visualize some of the flow features that were first found using the smearline visualization in figure 8. A combination of both kinds of visualizations gives the best understanding of how the flow behaves.

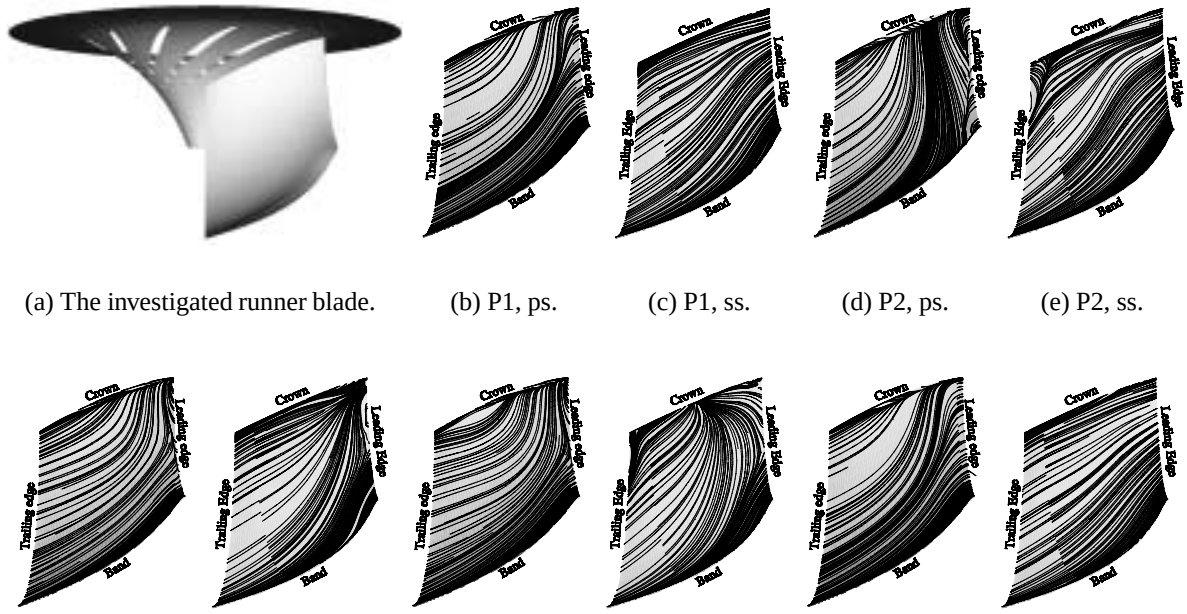

(a) The investigated runner blade. (b) P1, ps. (c) P1, ss. (d) P2, ps. (e) P2, ss.

(f) P3, ps. (g) P3, ss. (h) P4, ps. (i) P4, ss. (j) P5, ps. (k) P5, ss.

Figure 8: Smearlines at the GAMM runner blade pressure side (ps) and suction side (ss) surfaces at the investigated operating points.

NUMERICAL CONSIDERATIONS

The main features of the finite volume CALC-PMB (Parallel MultiBlock) [2, 5, 8] CFD code are its use of conformal block structured boundary fitted coordinates, a pressure correction scheme (SIMPLEC [3]), cartesian velocity components as the principal unknowns, and a collocated grid arrangement together with Rhie and Chow interpolation. The discretization schemes used in this work are a second-order Van Leer scheme for convection and a second-order central scheme for diffusion. The computational blocks are solved in parallel with Dirichlet-Dirichlet coupling using PVM (Parallel Virtual Machine) or MPI (Message Passing Interface). The parallel efficiency is excellent, with super scalar speedup for load balanced applications [7]. The ICEM CFD/CAE grid generator is used for grid generation and Ensight and Matlab are used for post-processing.

The correct solution is assumed to be reached when the largest normalized residual of the momentum equations, the continuity equation and the turbulence equations is reduced to 10^{-3}. The momentum equation residuals are normalized by the sum of the mass flow through the turbine and the mass flow through the periodic surfaces multiplied by the largest value of the velocity component of each equation. The continuity equation residual is normalized by the sum of the mass flow through the turbine and the mass flow through the periodic surfaces. The turbulence equations residuals are normalized by the largest residual during the iterations.

Acknowledgements

This work is financed and supported by ELFORSK (Swedish Electrical Utilities Research and Development Company), the Swedish National Energy Administration and GE Energy (Swe-

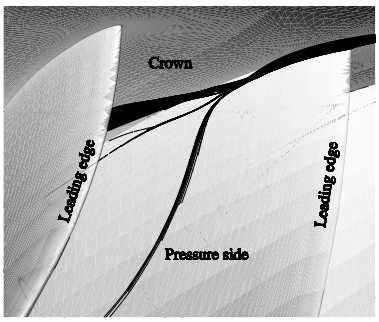

(a) Flow separation on the pressure side close to the crown. All operating points.

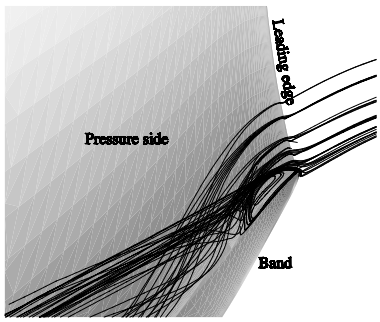

(b) Re-circulation at the leading edge pressure side, close to the band. Operating point 2.

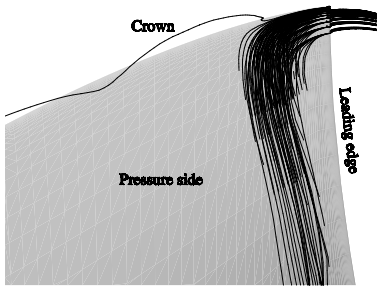

(c) Boundary layer streamlines, at the leading edge pressure side close to the crown, affected by centrifugal force. Operating point 2.

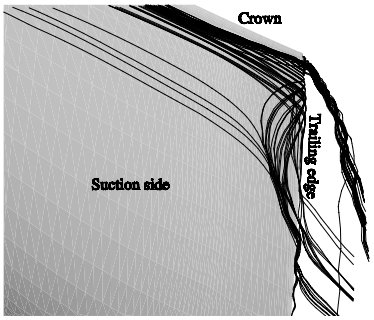

(d) Re-circulation, vortex rope and wake streamlines. Operating point 2 on the suction side close to the trailing edge and crown.

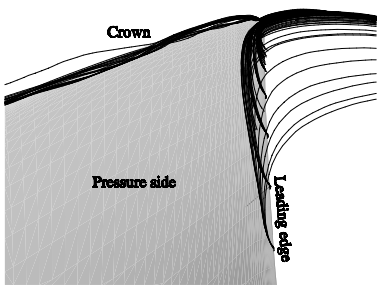

(e) Stagnation flow at the leading edge pressure side, close to the crown. Operating points 3 and 4.

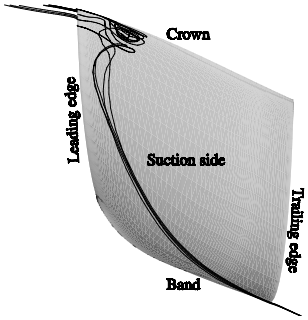

(f) Re-circulation at the leading edge suction side, close to the crown. Operating point 4.

Figure 9: GAMM flow feature visualization using streamlines.

den) AB.

GE Energy (Sweden) AB and its staff, particularly Bengt Nauclér, are gratefully acknowledged for their support and the information on geometry.

Professor F. Avellan and the staff at IMHEF-EPFL in Lausanne are gratefully acknowledged for their influence during the preliminary stages of this work and for making available the GAMM information.

The computational resources used at UNICC, Chalmers, are gratefully acknowledged.

References

[1] U. Andersson. Turbine 99 - Experiments on draft tube flow (test case T). In *Proceedings from Turbine 99 - Workshop on Draft Tube Flow*, 2000, ISSN: 1402 - 1536.

[2] L. Davidson and B. Farhanieh. CALC-BFC: A Finite-Volume Code Employing Collocated Variable Arrangement and Cartesian Velocity Components for Computation of Fluid Flow and Heat Transfer in Complex Three-Dimensional Geometries. Rept. 95/11, Thermo and Fluid Dynamics, Chalmers University of Technology, Gothenburg, 1995.

[3] J.P. Van Doormaal and G.D. Raithby. Enhancements of the SIMPLE method for predicting incompressible fluid flows. *Num. Heat Transfer*, 7:147–163, 1984.

[4] L. Gros, J.L. Kueny, F. Avellan, and L. Bellet. Numerical flow analysis of the GAMM turbine at nominal and off-design operating conditions. In *Proceedings of the XIX IAHR Symposium, Hydraulic Machinery and Cavitation*, pages 121–128, 1998.

[5] H. Nilsson. A Numerical Investigation of the Turbulent Flow in a Kaplan Water Turbine Runner. Thesis for the degree of Licentiate of Engineering 99/5, Dept. of Thermo and Fluid Dynamics, Chalmers University of Technology, Gothenburg, 1999.

[6] H. Nilsson. Numerical Investigations of Turbulent Flow in Water Turbines. Thesis for the degree of Doctor of Philosophy, to be defended in the autumn of 2002, Dept. of Thermo and Fluid Dynamics, Chalmers University of Technology, Gothenburg, 2002.

[7] H. Nilsson, S. Dahlström, and L. Davidson. Parallel multiblock CFD computations applied to industrial cases. In C.B. Jenssen *et al.*, editor, *Parallel Computational Fluid Dynamics - Trends and Applications*, pages 525–532. Elsevier Science B.V., 2001.

[8] H. Nilsson and L. Davidson. CALC-PVM: A parallel SIMPLEC multiblock solver for turbulent flow in complex domains. Int.rep. 98/12, Dept. of Thermo and Fluid Dynamics, Chalmers University of Technology, Gothenburg, 1998.

[9] H. Nilsson and L. Davidson. A numerical investigation of the flow in the wicket gate and runner of the Hölleforsen (Turbine 99) Kaplan turbine model. To be published. In *Proceedings from Turbine 99 II*, 2001.

[10] H. Nilsson and L. Davidson. A validation of parallel multiblock CFD against the GAMM Francis water turbine runner at best efficiency and off-design operating conditions. Int.rep. 01/02, Dept. of Thermo and Fluid Dynamics, Chalmers University of Technology, Gothenburg, 2001.

[11] H. Nilsson and L. Davidson. A general method for estimating numerical accuracy in swirling flow, submitted for publication. *Int. J. Fluids Eng.*, 2002.

[12] H. Nilsson and L. Davidson. Validations of finite volume CFD against detailed velocity and pressure measurements in water turbine runner flow, submitted for publication. *Int. J. Numer. Meth. Fluids*, 2002.

[13] O. Santal and F. Avellan. Hydraulic analysis of flow computation results. In *Proceedings of the 16th IAHR Symposium*, volume 2, pages 545 – 554, 1992.

[14] G. Sottas and I. L. Ryhming, editors. *3D-Computations of Incompressible Internal Flows - Proceedings of the GAMM Workshop at EPFL, September 1989, Lausanne - Notes on Numerical Fluid Mechanics*. Vieweg, Braunschweig, 1993.

[15] D.C. Wilcox. Reassessment of the scale-determining equation for advanced turbulence models. *AIAA J.*, 26(11):1299–1310, 1988.